

Temporal and Spatial Changes of Water Occurrence in the Selenga River Delta

Saeid Aminjafari¹, Ian Brown², Sergey Chalov³, Marc Simard⁴, Jerker Jarsjö¹, Mehdi Darvishi¹, and Fernando Jaramillo¹

¹Stockholm University

²University of Stockholm

³Faculty of Geography, M. V. Lomonosov Moscow State University

⁴Caltech/Jet Propulsion Laboratory

November 23, 2022

Abstract

Surface water occurrence in river deltas is governed by precipitation, evaporation, and the influx and outflux of water to and from the delta. Although studies of changes in water occurrence have been conducted at large scales, precise detection of changes in water occurrence is missing for most important river deltas. We take the case of the endorheic Selenga River Delta in Russia and train an accurate classification and quantification of water occurrence in its domain. We utilize remotely sensed observations of the Landsat satellite imagery during the last 33 years and implement supervised classification to map the surface water extent and its changes between periods of 1987-2002 and 2003-2019. We find that water occurrence has decreased in the Delta, with seasonally inundated areas presenting more pronounced decreases in water occurrence than permanent water bodies. We show that the change in the surface runoff is the main driver of changes in the spatial patterns of surface water with $R^2 = 0.58$, while changes in water level in the recipient Lake Baikal do not influence water occurrence in the Delta. Our results show that the shrinkage and expansion of the water surface reflect the change in the freshwater supply of the Delta, and the management of the Selenga River needs to consider the impact of changes on the water occurrence.

Temporal and Spatial Changes of Water Occurrence in the Selenga River Delta

Saeid Aminjafari¹, Ian Brown¹, Sergey Chalov², Marc Simard³, Jerker Jarsjö¹, Mehdi Darvishi¹, Fernando Jaramillo^{1,4}

¹Department of Physical Geography and Bolin Centre for Climate Research, Stockholm University, SE-106 91, Stockholm, Sweden.

²Faculty of Geography, Lomonosov Moscow State University, 119991 Moscow, Russia.

³Radar Science and Engineering Section, NASA Jet Propulsion Laboratory, USA.

⁴Baltic Sea Centre and Stockholm Resilience Center, Stockholm University, SE-106 91 Stockholm, Sweden.

Corresponding author: Saeid Aminjafari (saeed.aminjafari@natgeo.su.se)

Key Points:

- Water occurrence has decreased in the Selenga River Delta within the last three decades.
- The change in water occurrence correlates with the change in the river discharge, and not with the change in lake water level.
- The Change in river discharge and sediment discharge are changing the stream network of the Selenga River Delta.

25 **Abstract**

26 Surface water occurrence in river deltas is governed by precipitation, evaporation, and the influx
27 and outflux of water to and from the delta. Although studies of changes in water occurrence have
28 been conducted at large scales, precise detection of changes in water occurrence is missing for
29 most important river deltas. We take the case of the endorheic Selenga River Delta in Russia and
30 train an accurate classification and quantification of water occurrence in its domain. We utilize
31 remotely sensed observations of the Landsat satellite imagery during the last 33 years and
32 implement supervised classification to map the surface water extent and its changes between
33 periods of 1987-2002 and 2003-2019. We find that water occurrence has decreased in the Delta,
34 with seasonally inundated areas presenting more pronounced decreases in water occurrence than
35 permanent water bodies. We show that the change in the surface runoff is the main driver of
36 changes in the spatial patterns of surface water with $R^2 = 0.58$, while changes in water level in
37 the recipient Lake Baikal do not influence water occurrence in the Delta. Our results show that
38 the shrinkage and expansion of the water surface reflect the change in the freshwater supply of
39 the Delta, and the management of the Selenga River needs to consider the impact of changes on
40 the water occurrence.

41 **1 Introduction**

42 River deltas are responsible for ecosystem services to humans such as freshwater storage,
43 pollutant retention and attenuation, recreational activities, flood control, and fishing (Golden et
44 al., 2014; Guo et al., 2017; Lu & Kwoun, 2008). Despite their importance in providing these
45 services, they are now under pressure by effects from human development and greenhouse-gas
46 emission climate change. For instance, in-stream quarrying leads to sediment compaction due to
47 the extraction of the resources beneath the sediments. Upstream water impoundment and
48 regulation decreases sediment discharge and flattens runoff peaks necessary for hydraulic
49 flushing and wetland sheet flow (Syvitski et al., 2009). Change in water occurrence is an
50 indicator of such effects (Zhang et al., 2017). The term water occurrence is defined as the
51 presence of water on the specific location on the surface and in a particular moment in time. For
52 the particular case of deltas, water occurrence can be permanent in areas of open water such as
53 main river channels, streams, and in-stream wetlands, or temporary such as sand banks, flooded
54 wetlands and flood plains. Apart from the direct effects from human activities, changes in water

55 occurrence are also driven by in-stream hydraulics, fluvial geomorphologic processes and
56 sediment transport. The study of the changes in hydrological connectivity resulting from the
57 spatial and temporal distribution of water occurrence and the distribution of surface water
58 patches in the deltas are relevant for conservation of deltaic ecosystems and agricultural-
59 industrial activities (Cui et al., 2020; Nguyen et al., 2020), management of these water resources
60 and to strengthen their resilience to climatic and human-driven impacts and their functions as
61 biodiversity niches and ecosystem service providers (Borja et al., 2020).

62 Concerning the changes in the hydrology and morphology of the deltas irrespective of the
63 changes' direction, global estimations point to gains of roughly 54 square kilometers of land per
64 year due to land-use change and deforestation (Nienhuis et al., 2020). On the other hand, during
65 the last two decades, floods caused by heavy precipitation, river overflow, and storm surges have
66 submerged 260,000 km² in 85 percent of all deltas around the world (Syvitski et al., 2009).
67 Although these studies agree on the global expansion of the water surface, the magnitude of the
68 change depends on whether they have studied the seasonal and permanent water bodies
69 separately or together (Borja et al., 2020; Donchyts et al., 2016; Pekel et al., 2016). The change
70 in global surface water occurrence is spatially heterogeneous and its direction of change, loss or
71 gain, varies among deltas (Borja et al., 2020). For example, Zhang et al. (2017) detected 99
72 newly formed lakes and increased lake areas on the Tibetan Plateau from 1970 to 2013, as
73 opposed to what was found in the neighboring Mongolian Plateau during the same period where
74 208 lakes vanished and in 75% of the remaining lakes (Zhang et al., 2017). The studies
75 attempting to quantify changes in water occurrence at the global scale, although are very relevant
76 for the assessment of global water resources, lack a detailed understanding of local changes in
77 water occurrence, obviously pertaining the scale of the global scale of such assessments. They
78 also fail to recognize the main drivers of changes in water occurrence in each water resource,
79 mainly if these are climatic (i.e., changes in evaporation, runoff, sea level rise) or anthropogenic
80 (in-stream mining, drainage, infrastructure).

81 Giesen (2020) and Neinhuis et al. (2020) emphasize that regional focus on both small and larger
82 and more complex deltas such as the Niger, Huang He, Mekong, and the Ganges is necessary to
83 understand and manage the hydrological and morphological changes in deltas with greater global
84 impacts. They also justify the importance of local studies that aim to identify changes in water

85 occurrence in individual case studies of regionally important deltas providing a large set of
86 ecosystem services.

87 Furthermore, satellite observations and machine learning algorithms are usually used to
88 understand water occurrence and its changes (Allen & Pavelsky, 2018; Borja et al., 2020; Chini
89 et al., 2017; Donchyts et al., 2016; Guo et al., 2017; Pekel et al., 2016; Zhang et al., 2017). The
90 Landsat project, with more than 35 years of high-resolution acquisitions is a convenient source
91 of optical imagery to monitor change in water occurrence, with even several images available per
92 month for specific deltas. Advanced computational algorithms and cloud-based platforms enable
93 the processing of large amounts of data in relatively short periods, providing a high-spatial
94 resolution of changes in water occurrence. Unsupervised classification methodologies are usually
95 used to study long-term changes in global water occurrence (Borja et al., 2020; Donchyts et al.,
96 2016; Pekel et al., 2016), mostly without training data. Training data, or in other words using
97 pre-existing knowledge in the spatial distribution of water occurrence, would greatly improve the
98 prediction of water occurrence, and avoid misclassifications of water surfaces, as it sometimes
99 occurs with unsupervised classification methodologies.

100 We here use the case of the Selenga River Delta to address the three knowledge gaps mentioned;
101 1) to study changes in water occurrence with focus on deltas, 2) identifying the contribution of
102 hydroclimatic drivers to changes in water occurrence, and 3) applying training data to improve
103 the accuracy of the water-land delineation required to determine water occurrence. We apply this
104 method in the Selenga River Delta in Russia, an endorreic delta covering 540 km² and a water
105 resource that plays a key role in the ecosystem of the region and of Lake Baikal, the inland water
106 body receiving its waters. The delta has been experiencing a decrease in size that goes against
107 the global expansion of other water bodies (Borja et al., 2020; Donchyts et al., 2016; Pekel et al.,
108 2016).

109 **2 Materials and Methods**

110 **2.1 Study area**

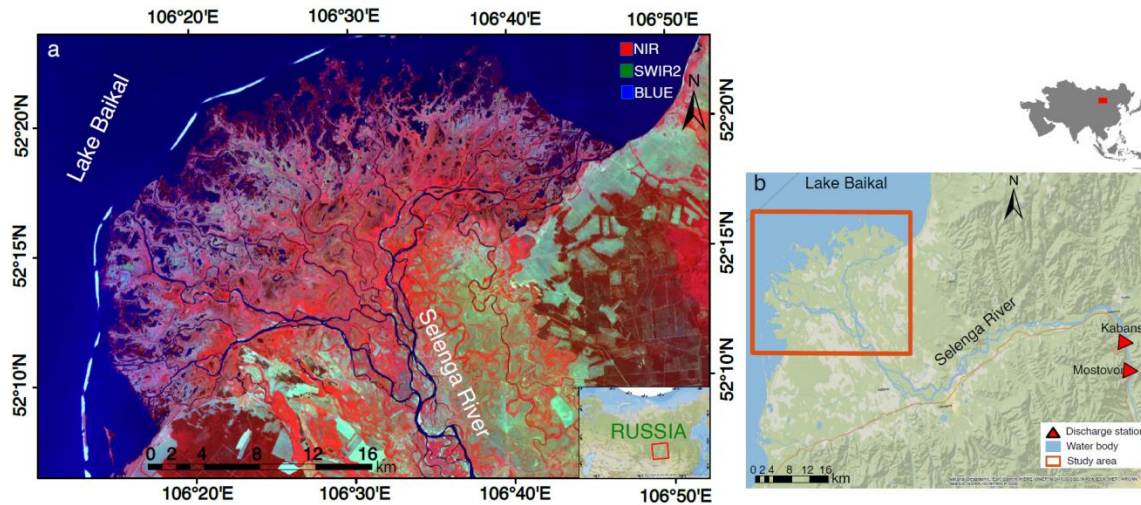
111 The Selenga River Delta is located in eastern Russia (Figure 1) along the southern shore
112 of Lake Baikal. Lake Baikal is the oldest (25 million years) and the deepest (~1800 meters) lake
113 in the world and a World Natural Heritage Site (UNESCO 1997). Lake Baikal contains

114 approximately 20% of all liquid fresh water on Earth (Berhane et al., 2018; Borisova, 2019). The
115 Selenga River is the main river flowing into Lake Baikal; one of around 365 other rivers. It is
116 responsible for almost 50% of the runoff water and 60% of the transported sediments into the
117 lake system, and its hydrological basin covers more than 82% of the Lake's basin (Berhane et al.,
118 2018). The unique habitats and ecosystem of the Selenga River Delta on Lake Baikal and its
119 purifying function have made this Delta a Ramsar wetland of international importance (Berhane
120 et al., 2018; Lane et al., 2015). The fan-shaped herbaceous wetland of the Selenga River Delta
121 covers an area of roughly 540 km² and receives mean annual precipitation of 315 mm (Figure
122 2b), concentrated from April to October and causing floods and freshets in the main channel and
123 tributaries, as reflected in the values of monthly runoff (Figure 2a). The arid continental climate
124 is described by temperature variations between +14°C on average in July and -19°C in January
125 permits a growing season of 140 to 150 days that starts in mid-May (Figure 2c), (Berhane et al.,
126 2018; Lane et al., 2015). Although the highest temperatures occur during the summer, the biggest
127 monthly temperature differences occur in the winter (bigger boxes and higher differences
128 between maximum and minimum).

129 The river faces several socioeconomic and environmental impacts which could, in turn,
130 impact Lake Baikal (Borisova, 2019). Being an endorheic river delta, changes in water
131 occurrence in this delta are not related to rising sea levels, but rather to hydroclimatic (Antokhina
132 et al., 2019) and fluvial geomorphological processes (Pietron et al., 2018; Dong et al., 2018;
133 Shinkareva et al., 2019). The anthropogenic impact on ecosystems in the Selenga River basin has
134 increased in the recent decades, e.g., by the extraction of minerals, primarily gold, urbanization,
135 and agricultural development, especially in the upper, Mongolian, part of the basin (Jarsjö et al.,
136 2017; Garmaev et al., 2019). The long-term low water period observed in the region (Gelfan &
137 Millionshchikova, 2018) has a significant impact on delta processes and wetland-dominated
138 areas of the Selenga Delta (Ghajarnia et al., 2020), also posing drastic changes in sediment
139 transport and water quality (Chalov et al., 2017b; Shinkareva et al., 2019).

140

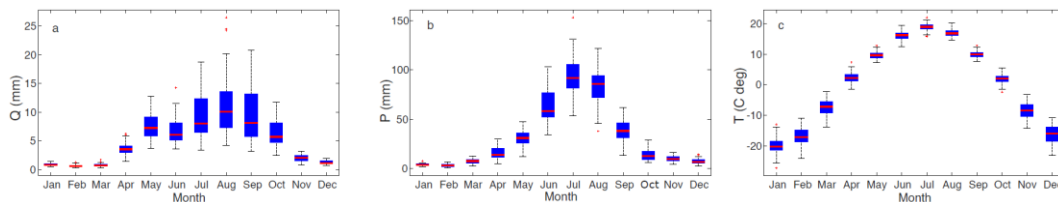
141



142

143 **Figure 1.** The Selenga River Delta. **a)** The location of the Selenga River Delta in Russia over a
 144 false-color Landsat 8 image acquired on 23 June 2017, path 132, frame 24. **b)** The location of the
 145 two discharge measuring stations used in this study (red triangles), roughly 100 km away from
 146 the Delta.

147



148

149 **Figure 1. Mean runoff, precipitation, and temperature.** Monthly box-whisker plots during the
 150 period 1985-2019 for **a)** Runoff (Q) in mm/month, **b)** precipitation (P) in mm/month, and **c)**
 151 temperature (T) in degrees centigrade. For the calculations of runoff, we divided discharge data
 152 at station Mostovoi by the upstream hydrological basin of 440,200 km², of which 67% falls in
 153 Mongolia and 33% in Russia.

154 2.2 Satellite data and classification

155 We mapped the occurrence of surface water in the Selenga River Delta in a time series of
 156 Landsat imagery. The classification data analyses were done using ENVI version 5.5 (Exelis
 157 Visual Information Solutions, Boulder, Colorado). We used Landsat Level-2 Surface Reflectance

158 data from the U.S. Geological Survey (Masek et al., 2006; Vermote et al., 2016, p. 8), which
 159 provides atmospherically corrected scenes of Landsat 4-5/TM, 7/ETM+, and 8/OLI upon request.
 160 In total, we obtained 195 images between 1987 and 2020 with less than 10% cloud cover over
 161 the scenes of the Selenga Delta but discarded more than half of the images due to Scan Line
 162 Corrector (SLC) errors (stripes on the Landsat-7 images due to instrument deficiency), cloud
 163 contamination, geometrical errors. Besides, several others acquired during winter were discarded
 164 since frozen water generates inaccurate classification results and unreliable water-land
 165 delineation. For the 87 remaining images, the Normalized Difference Vegetation Index (NDVI)
 166 and Normalized Difference Water Index (NDWI) were calculated by applying equation 1 and
 167 equation 2 (McFeeters, 1996), and stacked with Near Infrared (NIR), Shortwave Infrared
 168 (SWIR2) and the Blue band of each scene. The Red and Green represent the measured
 169 reflectance in the visible red band, and the visible green band of the spectrum, respectively.
 170 Since the highest reflectance difference between the water and the vegetation occurs in these
 171 bands and indices, using their combination in the classifier makes it possible to distinguish open
 172 water from the surrounding vegetation and land. Zhou et al. (2017) assessed the performance of
 173 different indices for differentiation of water surfaces and concluded that the NDWI-based
 174 algorithms (such as the one we used here) outperform other algorithms. However, classification
 175 methods might perform differently in different case studies (Zhou et al., 2017).

176

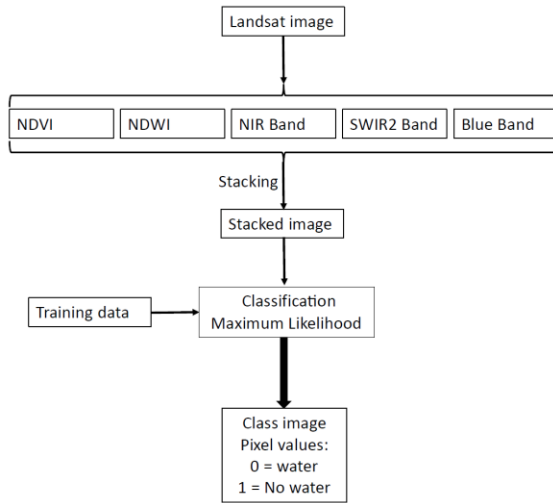
$$NDVI = \frac{NIR - Red}{NIR + Red} \quad \text{Equation 1}$$

177

$$NDWI = \frac{Green - NIR}{Green + NIR} \quad \text{Equation 2}$$

178 Before the supervised Maximum Likelihood classifier was applied on the stacked bands,
 179 we selected the training data of water surface recognition in each image by the visual inspection
 180 of the Google Earth's historical view on the corresponding date and the true-color composites of
 181 each scene (visible Red, Green, and Blue bands). We then applied the supervised Maximum
 182 Likelihood (ML) classifier on the stacked bands. The ML classification method is easy to

183 implement and has a fast processing procedure in comparison with other methods. The schematic
 184 process is shown in Figure 3.



185

186 **Figure 2.** Schematic flowchart for the land-water delineation process

187

188 We tested the accuracy of the classification when using the mentioned band-index
 189 combinations instead of only the available bands in Landsat products for four specific Landsat
 190 images and found that water surface classification is indeed improved (Tables S1 to S4,
 191 Supplementary materials). Based on visual inspections, we prepared two sets of land-water data;
 192 one for training the classifier and the other one for calculating the confusion Matrix and the
 193 classification accuracy. To avoid misinterpretation, we chose the land-water data sets in similar
 194 areas for all images as long as the delineation borders fitted the exact true-color locations of the
 195 water bodies.

196 The Maximum Likelihood supervised classifier is widely applied to satellite imagery for
 197 land cover mapping. Based on the training data, this algorithm assumes that the pixel classes are
 198 normally distributed in the spectral space and calculates the probability of a pixel belonging to a
 199 specific landcover class (c_m) (Richards, 1999) when the probability (p) of a pixel with a given
 200 value (d) of belonging to c_m is higher than the probability of belonging to any other class c_n
 201 (Richards, 1999) (equation 3).

202

$$d \in c_m \text{ if } p(c_m|d) > p(c_n|d) \text{ for all } n \neq m \quad \text{Equation 3}$$

203 2.3 Surface water occurrence and its changes

204 For each image and date, we classified each pixel binarily based on the results from the
 205 supervised Maximum Likelihood classifier, either zero or one; representing the existence or non-
 206 existence of surface water, respectively. Since only two classes are considered in the
 207 calculations, the non-vegetation dry lands might be misclassified with the pixels identified as
 208 water. To avoid this problem, we included the sand bars and other non-vegetation dry areas in
 209 training data as much as possible. To be able to compare the water occurrence time series with
 210 that of runoff from the main channel of the Selenga River and the lake levels of the Lake Baikal
 211 we need a single value of water occurrence for each image. To get that value, we spatially
 212 average the water occurrence of all pixels in a particular image. Therefore, we obtain the mean
 213 water occurrence for each image (\bar{w}_s : subscript s represents the spatial mean) as:

$$\bar{w}_s = \frac{\sum_{i=1}^r v_{i,j}}{r} \quad \text{Equation 4}$$

214 where $v_{i,j}$ is the water occurrence of the i^{th} pixel in the class image j with the total number
 215 of pixels r .

216 We followed a published methodology (Pekel et al., 2016) that estimates water
 217 occurrence on a given land surface to quantify the occurrence of water in the Selenga River Delta
 218 during the 33 years of the period 1987-2019. To obtain the water occurrence during the entire
 219 33-year period, we calculated for each pixel the mean of the binary values of all images for that
 220 specific pixel, leading to a final value between zero and one. Since not all months have the same
 221 number of images available, our interpretation of water occurrence is more biased towards the
 222 summer and autumn periods that contain more images due to favorable meteorological
 223 conditions than the other seasons. To draw unbiased conclusions, we calculated a mean value of
 224 water occurrence for each month in each pixel during the same period (w_m) as follows:

225

$$w_m = \frac{\sum_{j=1}^n v_{i,j}}{n} \quad \text{Equation 5}$$

226 where m is the month, j is a class image from the total of class images available for that
 227 specific month (n) from January 1987 to December 2019. While images taken in the summer and
 228 autumn periods have a higher quality and have a lower presence of clouds, images taken during
 229 the months of December, January, and February were discarded as the Lake Baikal and some
 230 parts of the Delta are covered by ice and snow, affecting the analysis of water occurrence.
 231 Moreover, we excluded the change in water occurrence of March since there is only one class
 232 image in March (located in the first period).

233 The mean water occurrence in each pixel and for the whole period (\bar{w}) is calculated by
 234 averaging the water occurrence of all months (w_m) as:

$$\bar{w} = \frac{\sum_{m=1}^{n=12} w_m}{12} \quad \text{Equation 6}$$

235 In order to understand the temporal change in water occurrence for each month of the
 236 year (Δw_m), we subtracted the mean w_m of the period 1987-2002 (w_{m1}) from that of the period
 237 2003-2019 (w_{m2}) as:

238

$$\Delta w_m = w_{m2} - w_{m1} \quad \text{Equation 7}$$

239 Finally, the mean change of water occurrence ($\overline{\Delta w}$) per pixel was calculated by averaging
 240 the monthly changes of water occurrence Δw_m as:

241

$$\overline{\Delta w} = \frac{\sum_{m=1}^{n=12} \Delta w_m}{12} \quad \text{Equation 8}$$

242 As w_m ranges from zero to one, Δw_m and $\overline{\Delta w}$ do from -1 to +1, where a value of -1
 243 means that the pixel did not contain water in any of the class images in the second period and
 244 contained water in all class images in the first period, and vice versa. Therefore, $\overline{\Delta w}$ provides
 245 information about the expansion and shrinkage of water surface area; the negative and positive
 246 values correspond to decreasing and increasing water occurrence, respectively. All of the raster
 247 calculations and visualizations were performed in the ArcGIS environment and MATLAB
 248 R2018a. Finally, we divided the Delta in three different regions of analysis (R1, R2, and R3,

249 respectively; Figure 4) to identify the two main drivers of water surface occurrence: 1)
250 Oscillations of lake water level and 2) upstream water supply by main river discharge.

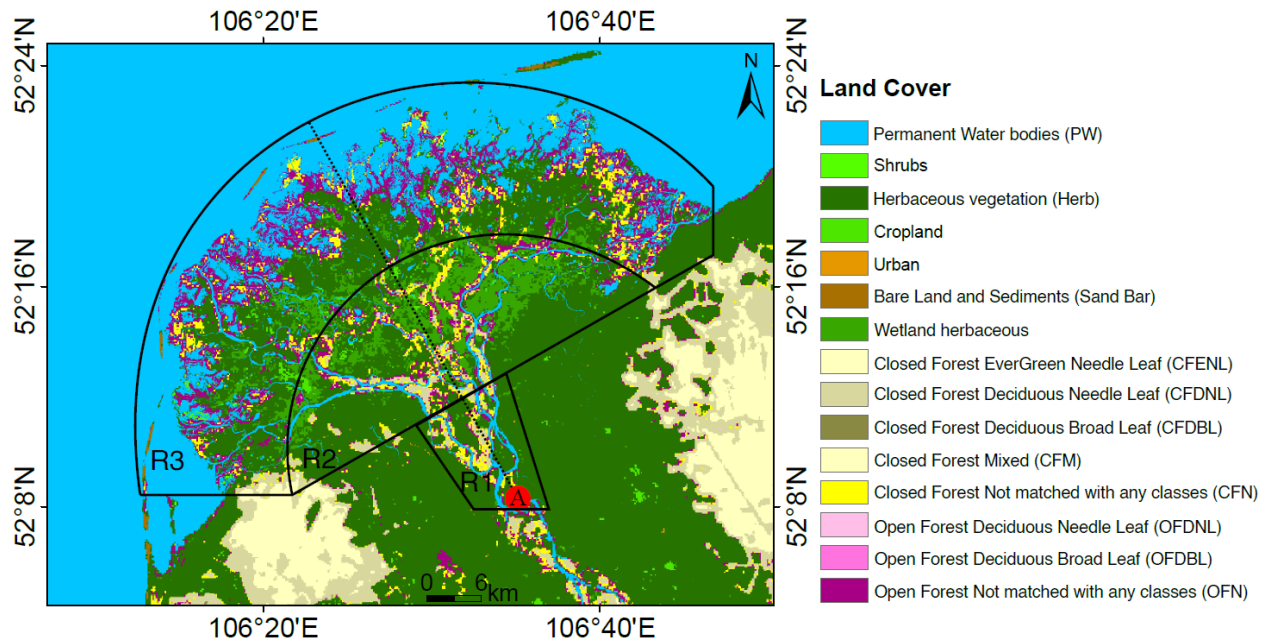
251 2.4 Hydroclimatic data and landcover map

252 We analyzed the dependence of surface water occurrence in the Delta on two
253 hydrological variables: The Selenga River's surface runoff and water level in the Lake Baikal.
254 For the first, we used daily discharge data from the Russian Federal Service for
255 Hydrometeorology and Environmental Monitoring (Roshydromet) in the gauging stations closest
256 to the Delta (Mostovoi and Kabansk stations), both located approximately 100 km upstream of
257 the Delta. We also extracted temperature and precipitation data for the region of the Delta from
258 the gridded data sets of the CRU of the Climatic Research Unit (Hulme, 1992; Hulme et al.,
259 1998). Both data sets have $0.5^\circ \times 0.5^\circ$ grids, with monthly data available from 1901 to 2018. For
260 the case of precipitation, we used the mean monthly precipitation values of all cells fallen into
261 the Selenga River basins upstream of each of the two discharge stations. To make surface water
262 occurrence and runoff data comparable, we calculated the ten- and five-day averages of runoff
263 data before, after, and on the acquisition date and time of the images.

264 For Lake Baikal water level, we used two gauge stations of the International Data Centre
265 on Hydrology of Lakes and Reservoirs (Hydrolare) from 1963 to 2015, one roughly 60 km
266 southwest of the Delta (coastal Babushkin station) and another one in the middle part of the Lake
267 (Ushkanij station), together with the processed satellite altimetric data of the Hydroweb service
268 (Crétaux et al., 2011) available since 1992 and continuously updated. The altimeters used in this
269 dataset are Topex-Poseidon, Jason, Jason-2, Jason-3, and Sentinel-3A, and the point of
270 observation is in the middle of the lake and near to the Ushkanij gauge station, which is roughly
271 200 km away from the Delta. Before 2014, the temporal resolution of this dataset was over ten
272 days, and since 2014 new altimetric satellites have been launched in the orbits, giving one-day
273 resolution water level data.

274 We further studied water occurrence and its changes in the different land cover
275 ecosystems present in the Delta, such as permanent water bodies, seasonally inundated areas, and
276 lands, wetlands, and forests (Figure 4). We preliminarily assigned a landcover category to each
277 pixel based on their \bar{w} values; pixels with $\bar{w} > 80\%$ falling into the permanent water category,
278 pixels with $\bar{w} < 10\%$ into dry lands and between $10\% < \bar{w} < 80\%$ as seasonal water bodies. We

279 merged this preliminary water occurrence categorization with the dynamic land cover map of the
 280 Copernicus Global Land Service at 100-m resolution (CGLS-LC100) (Buchhorn et al., 2019)
 281 (Fig. 4). This product, obtained via Google Earth Engine, has global coverage and its reference
 282 year is 2015.



283

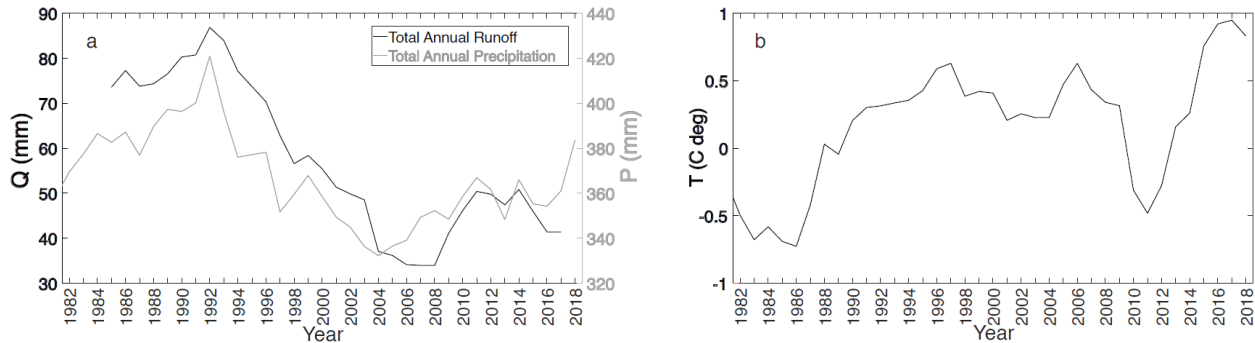
284 **Figure 3. Land cover (CGLS-LC100) and three regions of focus in the Delta.** The closest
 285 upstream borders of R2 and R3 are 10- and 20-km downstream from point A along the dashed
 286 line, respectively.

287 3 Results

288 Precipitation and runoff in the Selenga River Basin (area = 445,000 km²) have decreased
 289 during the period 1987-2019, with a consistent drop from the highest reported peak in 1992 to its
 290 lowest been 2004 and 2008. Air temperature in the Delta increased to the highest mean annual
 291 values in 2016 and 2017 (Figure 5). The map of mean water occurrence \bar{w} (Figure 6) visualizes
 292 the stream network and the areas susceptible to seasonal flooding. As expected, areas along the
 293 coast of the Lake Baikal have a higher water occurrence than those inland. The change in water
 294 occurrence between the two periods $\Delta\bar{w}$ (Figure 7) shows the expansion and shrinkage of the
 295 surface water areas attributed to river planform migration, newly formed or dried out streams and
 296 lakes, and the flooding of flood-prone areas. The supplementary table S5 shows the number of
 297 images per month and year used to produce the map of water occurrence and its changes. In

298 general, negative values of $\overline{\Delta w}$ (red in Figure 7) are dominant across the Delta and concentrated
 299 in the southwest and eastern sections, where the water extent has mostly decreased.

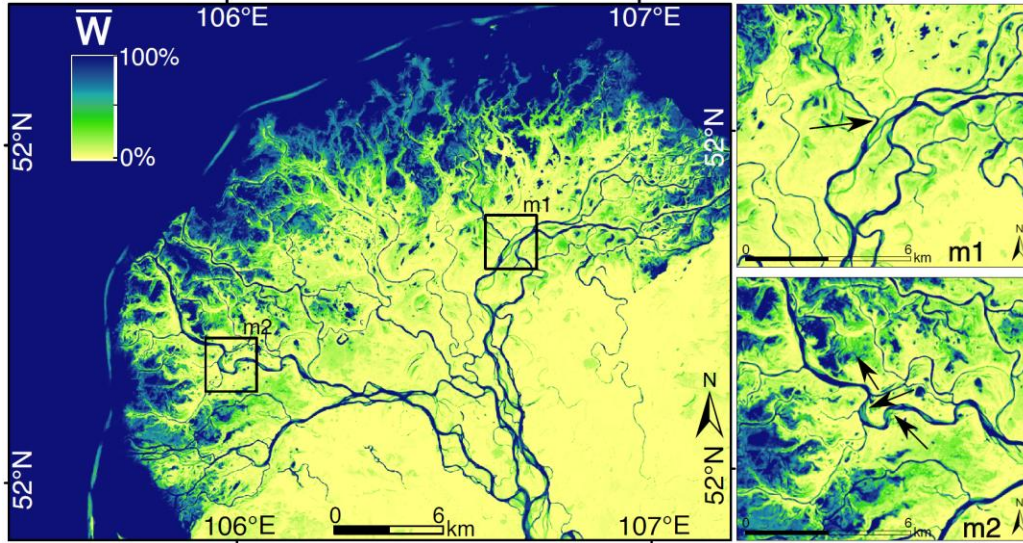
300



301

302 **Figure 4. The time series of Runoff (Q), Precipitation (P), and Temperature (T) in the**
 303 **Selenga River hydrological basin. a) the 5-year moving average of total annual P on the right**
 304 **axis and Q on the left axis. b) the 5-year moving average of T.**

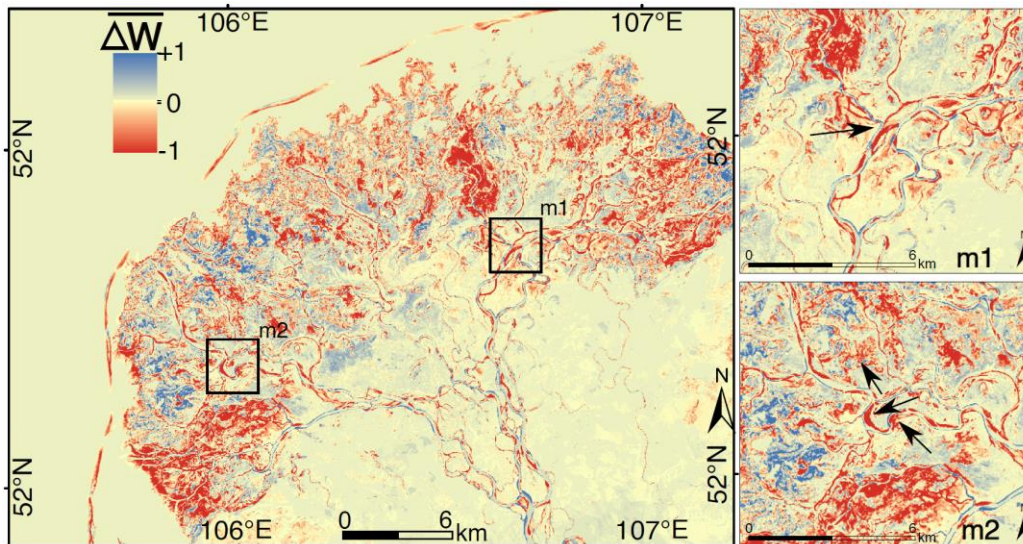
305 A first look into the spatial distribution of $\overline{\Delta w}$ highlights a decreased water occurrence in
 306 the outer sediment banks in the proximity of Lake Baikal due to the accumulation of sediments
 307 and a decline in coverage of surface water (Figure 7). Decreasing $\overline{\Delta w}$ in close vicinity of the
 308 main channel and streams' bends shows instead river planform migration as sand and grabble
 309 areas are uncovered. Water occurrence \bar{w} shows for example two possible paths of a river
 310 branch (e.g., panel m1 in Figures 6 and 7). The availability of the images does not allow to
 311 determine the specific day when the change in river course took place; however, the class images
 312 available between 1999 and 2001 show the traces of the newly-formed path. Additionally, the
 313 change Δw hints which is the old (north-eastern direction) and new (north-western direction)
 314 path, due to changes in water occurrence. The same analysis in panel m2 points instead to the
 315 presence of river bends and temporary water bodies, in which \bar{w} is still high but less than that of
 316 permanent water bodies. Also, when $\overline{\Delta w}$ is high (close to -1 or +1) it shows where in the river
 317 network are meandering processes occurring and when can these lead to oxbow lake formation in
 318 the future.



319

320 **Figure 6. Mean Surface water occurrence (\bar{w}) in 1987–2019.** Pixels not holding water in any
 321 of the class images are in yellow (0%) and pixels that hold water in all class images in dark blue
 322 (100%). The arrow in zoom panel m1 shows a change in river course. The arrows in zoom panel
 323 m2 show river bends and flood-prone areas with high water occurrence but still less than that of
 324 permanent water bodies.

325

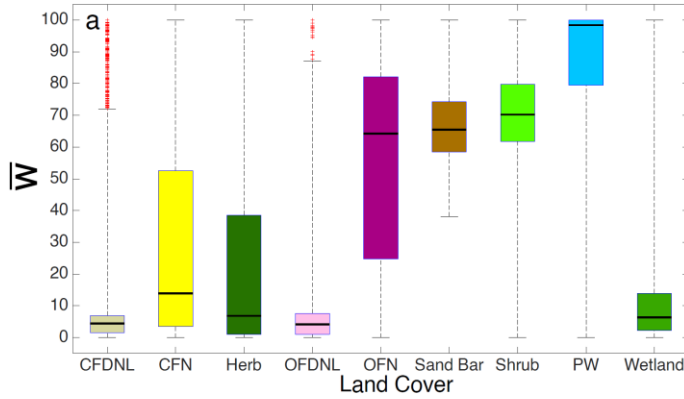


326

327 **Figure 7. Change in surface water occurrence ($\overline{\Delta w}$) between 1987-2002 and 2003-2019.**
328 Red areas (-1) show loss of water surface and blue areas a gain (+1).

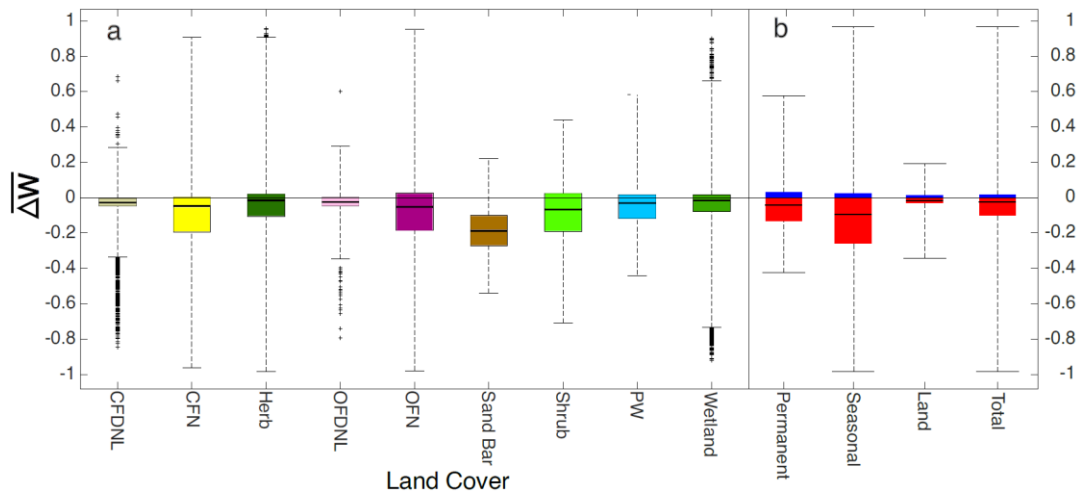
329 Based on the CGLS-LC100 landcover map shown in Figure 4, we summarized the
330 distribution of \bar{w} and $\overline{\Delta w}$ for each landcover (Figure 8 and Figure 9a). In general, there is a
331 decrease in water occurrence throughout the Delta. The decrease in water occurrence is more
332 recurrent in seasonally flooded areas and even larger than the decrease in permanent water
333 bodies (Figure 9.b). By dividing the number of pixels in which the water occurrence has changed
334 by the total number of pixels available in each category, we show that the mean water occurrence
335 in the permanent water bodies changed only in 20% of the pixels, while in seasonally flooded
336 water it did in 90% of the pixels. The number of pixels is presented in the supplementary table
337 S6.

338 In the permanent water bodies of the river channel, $\overline{\Delta w}$ varies between -0.17 and +0.08,
339 with the increasing water occurrence located near the river bends (green colors in Figure 6).
340 Although \bar{w} in the outer bank of the Delta (the sand bar near the Lake) is larger than 60%, the
341 negative values of $\overline{\Delta w}$ confirm a decrease in water occurrence as the sand bars have become
342 thicker during the last three decades. The \bar{w} in closed and open forests with needle-leaf trees
343 (CFDNL and OFDNL) and perennial woody crops is less than 10% and is fairly constant.
344 However, due to the canopy coverage in these regions and the limitations of Landsat products, it
345 is not always possible to monitor the surface water beneath the tree canopy. The largest values of
346 \bar{w} are found in areas covered by herbaceous vegetation (Herb) and shrubs (the plants that are less
347 than five meters tall) such as the wetland-dominated areas and in the proximity of the river
348 network, as they are more susceptible to river overflow (Figure 9a). Although in areas covered
349 by shrubs, the water occurs in more than 60% of the images, there is a general shrinkage of the
350 water surface in the majority of the pixels in these land covers (Figure 9a). Although this implies
351 that these areas are flooded less frequently in the second period than they were in the first period,
352 we cannot rule out the cause of an increase in the vegetation canopy due to the sensibility of
353 Landsat products to vegetation growth.



354

355 **Figure 8.** The distribution of \bar{w} for each land cover, with colors and acronyms corresponding to
 356 Figure 4.



357

358 **Figure 9.** The distribution of $\overline{\Delta w}$ **a)** for each land cover and **b)** permanent water, seasonal water,
 359 and land categories.

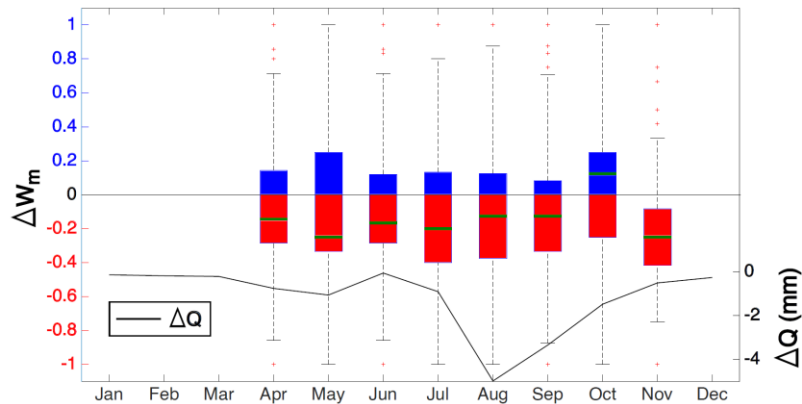
360 Supplementary Figure S1 shows the scatter plot of the monthly average of NDVI versus
 361 the monthly average of water occurrence and it can be seen that a significant linear regression
 362 exists between these two parameters. Thus, by increasing NDVI in the growing season (June to
 363 August) the water occurrence decreases.

364 3.1 Relation of water occurrence to runoff and water level in Lake Baikal

365 The distributions of mean change in monthly water occurrence Δw_m between the periods
 366 1987-2002 and 2003-2019 for all the pixels (where $\Delta w_m \neq 0$) within the total area of the
 367 Selenga River Delta (i.e., R1+R2+R3) are shown in Figure 10 along with the change in monthly

368 runoff (ΔQ) in station Kabansk. The \bar{w} has mostly decreased in all months but October, as the
 369 median of the Δw_m the distributions are negative, agreeing with a generic decrease in runoff
 370 throughout all months and most notorious in August. Runoff instead has decreased the most in
 371 the month of August. Interestingly, the month of October sees the greatest number of pixels
 372 showing an increase in w_m , while the following month, November, sees the second smallest
 373 decrease in Q .

374



375

376 **Figure 10.** Monthly distributions of change in water occurrence (Δw_m) and runoff (ΔQ) between
 377 the periods 1987-2002 and 2003-2019 for the area of the Selenga River Delta (R1, R2, and R3).

378

379 In order to determine if changes in water occurrence \bar{w}_s in the Selenga River Delta were
 380 more related to changes in the lake or the river, we calculated the R^2 and statistical significance
 381 value ($p < 0.05$; Pearson) of the linear regression between \bar{w}_s and Q (and water level (WL) in the
 382 lake). We find a positive and significant ($p < 0.05$) linear regression between Q and \bar{w}_s that is
 383 significant in all three regions and highest ($R^2=0.58$) in the mid-region R2. The most relevant
 384 changes in water occurrence in the Delta seem to also replicate those in the Q series of the
 385 Selenga River, for example, the peaks of 1995, 1998, and 2014, after applying a LOESS filter to
 386 the time series (locally estimated scatterplot smoothing), as data points are not spread uniformly in
 387 time due to image availability (Figure 11a). This result is found regardless of the discharge
 388 station selected and different temporal moving windows of Q (i.e., instantaneous and 5-day and
 389 10-day averages of Q before and after the images' acquisition dates). In contrast, the lake water
 390 level does not influence the water occurrence of the class images, as all R^2 values are very low,

391 signaling a low influence of the backwater effect of the Lake on water occurrence in the Delta
 392 (Figure 11b, S2-S3).

393 **Table 1**

394 *Linear Regression Between \bar{w}_s and I) Runoff (Q) and II) Water Level (WL) in Lake Baikal, for*
 395 *Three Regions R1, R2 and R3.*

396

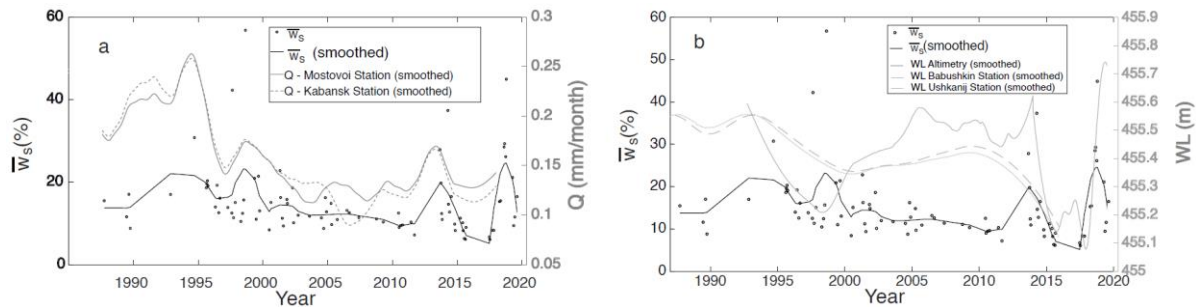
	\bar{w}_s vs. Q		\bar{w}_s vs. WL (Altimetry)	
	R ²	p-value	R ²	p-value
Region 1	0.213	3.13e-05	0.0026	0.644
Region 2	0.58	2.22e-15	0.0591	0.0268
Region 3	0.0791	0.0145	0.0004	0.864
Entire Delta	0.0222	0.202	0.0028	0.635

397

398 *Note.* Bold values are the highest of all regions. The surface runoff data are selected on
 399 the images' acquisition days, and the Lake water levels are nearest to the date of acquisitions.

400

401



402

403 **Figure 11.** The relationship between \bar{w}_s (left vertical axis) and **a) Q** and **b) Water Level** in Lake
 404 Baikal in region R2 (right vertical axis). Lines represent a Loess filter. The surface of reference

405 for the gauge stations is the sea level and for the altimetric water levels is geoid GGMO2C
406 (Tapley et al., 2005).

407 **4 Discussion**

408 We have found a net decrease in surface water occurrence in the Selenga River Delta
409 within the period 1987-2019 which agrees with a recent finding of a general decrease in water
410 occurrence in Norther Siberia (Borja et al., 2020), with both permanent and seasonal flooded
411 areas considered in both studies. Borja et al. (2020) also found that most decreases in surface
412 water area occurred in areas of seasonal flooding due to decreasing discharge in the rivers after
413 1997. On the other hand, studies that have not considered seasonally flooded areas show
414 different magnitude of changes in water occurrence. Pekel et al. (2016) and Donchyts et al.
415 (2016) found a global net increase in water occurrence, but the latter found a smaller expansion
416 of water surface than the former by taking into account only permanent water bodies (Borja et
417 al., 2020; Donchyts et al., 2016; Pekel et al., 2016).

418 Moreover, different periods of analysis yield different results of changes in water
419 occurrence. For example, Borja et al. (2020) showed that two periods of 1985-2000 vs 2001-
420 2015 and 1985-2005 vs 2013-2015 led to different magnitudes of a global increase in water
421 occurrence while Pekel et al. (2016) and Donchyts et al. (2016) studied the periods of 1985-1997
422 vs 1998-2005 and 1985-2005 vs 2013-2015, respectively, to find different magnitudes of
423 increased water occurrence.

424 We find in the case of the Selenga River Delta, that changes in water occurrence are more
425 related to changes in upstream runoff ($R^2=0.58$) rather than changes in water level in the lake
426 ($R^2=0.05$). This is probably due to the water budget in the Delta arising from the variability of
427 discharge, as water enters the delta, is temporarily stored within its boundaries to be later
428 discharged into Lake Baikal. In addition, the Selenga River has not been regulated by flow
429 divergence or dam construction. Other unregulated deltas and upstream rivers have also shown
430 high correlations between changes in water level and upstream discharge (Palomino-Ángel et al.,
431 2019). On the contrary, Jaramillo et al. (2018) found that in the case of the Magdalena River
432 Delta in Colombia, the relationship between water level change and change in upstream river
433 discharge was much lower ($R^2=0.17$) due to the regulation of freshwater into the Delta.

434 The relationship between water occurrence and upstream runoff should be theoretically
435 higher, as the Selenga River is the only freshwater input into the Delta. More water discharge
436 brings more sediment loads, that when accumulated, leading to a gain in dry surfaces. It is
437 known that the Delta retains ~3000 tons/day of suspended sediments, an amount that outweighs
438 the total flux of sediments to the entire Lake (Chalov et al., 2015). However, this may not be the
439 case for the Selenga River delta under the period of study. Chalov et al. (2015) found that during
440 the period 1983-2011 the correlation factor between the surface runoff and the suspended
441 sediment concentration was only 0.16 (Chalov et al., 2015; Moragoda & Cohen, 2020).
442 Furthermore, no significant overbank flow has been observed in the flood season after 2011
443 (Chalov et al., 2015), leading to no flooding from bank overflow, reducing an even stronger
444 relationship between discharge and water occurrence.

445 On the other hand, the weak relationship between water occurrence and water level in
446 Lake Baikal is due to the fact that water levels of Lake Baikal are currently regulated by the
447 Irkutsk dam on the main outflow of Lake Baikal – Angara River. Since the Irkutsk dam was
448 created in 1959, lake water levels are more homogeneous than before (during the last three
449 decades are within half a meter), and such changes may not imply considerable changes in water
450 occurrence in the Delta.

451 The results of a study published in 2020 indicate that 1000 deltas show a net land gain of
452 $54 \pm 12 \text{ km}^2$ per year (Nienhuis et al., 2020). Although the deltas studied herein are wave, tide,
453 and river-dominated and are affected by the sea-level rise, the authors showed that deforestation
454 is responsible for such gain of land area in the Deltas. In the case of the Selenga River Delta, a
455 decrease in water occurrence (water surface shrinkage) intensifies the effect of the land gain.

456 Our results also show that the change in water occurrence is not heterogeneous
457 throughout the Delta. The spatial percentage of the shrinkage of the water surface (in the R2
458 region) in the left, right, and the middle part of the Delta is 44%, 51%, and 52%, respectively.
459 These results are consistent with the findings in Chalov et al., (2017a) that show the maximum
460 lift between 1956 and 1998 happened in the right and the middle side of the Delta, and more
461 recently some water bodies are filled with sediment that contributed to the growth of the Delta.
462 Their estimation shows higher relative suspended sediment retention in the middle and the right
463 side of the Delta (Chalov et al., 2017a). Although the sediment discharge is decreasing in the

464 area, the surface of the Delta is rising by a velocity of 75 cm/year (Chalov et al., 2017a). In terms
465 of the longitudinal change of the water occurrence, the spatial percentage of the water loss in
466 regions R1(River bifurcation), R2(wetland-dominated area), and R3 (closer to the Lake) are
467 0.41%, 0.49%, and 45% respectively. These results show that wetland-dominated areas with low
468 elevations are more influenced by river and lake water levels.

469 **5 Conclusions**

470 The spatial distribution of changes in water surface in the Selenga River Delta relate to
471 inputs of freshwater and sediment into the Delta, which are important for the urban, agricultural,
472 and industrial use, and the ecology of the Delta. We find that:

473 1. The mean water occurrence in the Selenga River Delta decreased between 1987-2002
474 and 2003-2019. The decreasing water occurrence is mostly in seasonally flooded regions rather
475 than in permanent water bodies. The outer bank of the Delta, the border of the Lake and the
476 Delta, have gained land probably by sediment accumulation. The largest changes in water
477 occurrence are mostly seen along the mainstream bends due to planform migration, and
478 highlighted by the case of a change in direction of the river course in the east of the Delta.

479 2. There is a significant relationship between water occurrence and the surface runoff.
480 The best fit between these two parameters was observed for the inner zone of the Delta with an
481 R^2 of 0.58. On the contrary, water occurrence does not correlate with the Lake water level.

482 3. We have improved the common methodology of determining water occurrence by
483 providing the training data for all of the available images in Maximum Likelihood supervised
484 classification.

485 The change in water occurrence between 1987-2002 and 2003-2019 shows that river
486 planforms, stream networks, and consequently the shape of the Delta are changing due to
487 changes in river discharge. We expect that any modification of the river flow through upstream
488 damming and water diversion compounded by climate change will significantly impact the
489 Selenga River Delta.

490 **6 Acknowledgements and Data Accessibility**

491 The project was funded by Swedish Research Council for Environment, Agricultural
492 Sciences and Spatial Planning FORMAS (942–2015-740), and the Swedish National Space
493 Agency (180/18).

494 SCH was supported by Russian Fund for Basic research project 18-05-80094 and 19-05-
495 50109.

496 The Landsat Level-2 Surface Reflectance data were obtained from the U.S. Geological
497 Survey (<https://earthexplorer.usgs.gov/>) and are freely available On-demand. They are described
498 in these citation references: Masek et al. (2006), Vermote et al. (2016), p. 8. Digital Object
499 Identifier (DOI) for L8, L7 and L4 data respectively: [<https://doi.org/10.5066/F78S4MZJ>],
500 [<https://doi.org/10.5066/F7Q52MNK>], [<https://doi.org/10.5066/F7KD1VZ9>].

501 The temperature and precipitation data for the region of the delta were obtained from the
502 gridded data sets of the CRU of the Climatic Research Unit and are available in these in-text data
503 citation references: Hulme (1992) [with Open Database License:
504 <http://opendatacommons.org/licenses/odbl/1.0/> and Database Contents License:
505 <http://opendatacommons.org/licenses/dbcl/1.0/> under conditions of Attribution and Share-Alike:
506 <http://opendatacommons.org/licenses/odbl/summary/>], Hulme et al. (1998).

507 The dynamic land cover map of the Copernicus Global Land Service at 100-m resolution
508 (CGLS-LC100) is available at this in-text citation reference: Buchhorn et al. 2019.

509 For Lake Baikal water level, we used two gauge stations of the International Data Centre
510 on Hydrology of Lakes and Reservoirs (Hydrolare) from 1963 to 2015, Babushkin station and
511 Ushkanij station, together with the processed satellite altimetric data of the Hydroweb service
512 (Crétaux et al., 2011) available since 1992 and continuously updated.

513 The daily discharge data were obtained from the Russian Federal Service for
514 Hydrometeorology and Environmental Monitoring (Roshydromet) in the gauging stations closest
515 to the Delta (Mostovoi and Kabansk stations) and are not accessible to the public or research
516 community.

517 **References**

- 518 Allen, G. H., & Pavelsky, T. M. (2018). Global extent of rivers and streams. *Science*, *361*(6402),
519 585–588. <https://doi.org/10.1126/science.aat0636>
- 520 Antokhina, O.Y., Latysheva, I.V., Mordvinov, V.I. (2019). A case study of Mongolian
521 Cyclogenesis during the July 2018 blocking events. *Geogr. Environ. Sustain. Geography,*
522 *Environment, Sustainability*, *12*(3), pp.66-78. [https://doi.org/10.24057/2071-9388-2019-](https://doi.org/10.24057/2071-9388-2019-14)
523 14
- 524
- 525 Berhane, T. M., Lane, C. R., Wu, Q., Autrey, B. C., Anenkhonov, O. A., Chepinoga, V. V., &
526 Liu, H. (2018). Decision-tree, rule-based, and random forest classification of high-
527 resolution multispectral imagery for wetland mapping and inventory. *Remote Sensing,*
528 *10*(4), 580. <https://doi.org/10.3390/rs10040580>
- 529 Borisova, T. A. (2019). The evaluation of natural risks of floods in the Delta of the River
530 Selenga and engineering protection against flooding. In *IOP Conference Series: Earth*
531 *and Environmental Science* (Vol. 272, p. 022232). [https://doi.org/doi:10.1088/1755-](https://doi.org/doi:10.1088/1755-1315/272/2/022232)
532 1315/272/2/022232
- 533 Borja, S., Kalantari, Z., & Destouni, G. (2020). Global wetting by seasonal surface water over
534 the last decades. *Earth's Future*, *8*(3), e2019EF001449.
535 <https://doi.org/10.1029/2019EF001449>
- 536 Buchhorn, M., Smets, B., Bertels, L., Lesiv, M., Tsendbazar, N. E., Herold, M., & Fritz, S.
537 (2019). Copernicus global land service: Land Cover 100m: Epoch 2015: Globe. *Version*
538 *V2. 0.2*. <https://doi.org/10.5281/zenodo.3243509>
- 539 Chalov, S., Jarsjö, J., Kasimov, N. S., O. Romanchenko, A., Pietroń, J., Thorslund, J., &
540 Promakhova, E. V. (2015). Spatio-temporal variation of sediment transport in the Selenga
541 River Basin, Mongolia and Russia. *Environmental Earth Sciences*, *73*(2), 663–680.
542 <https://doi.org/10.1007/s12665-014-3106-z>
- 543 Chalov, S., Thorslund, J., Kasimov, N., Aybullatov, D., Ilyicheva, E., Karthe, D., et al. (2017a).
544 The Selenga River Delta: A geochemical barrier protecting Lake Baikal waters. *Regional*
545 *Environmental Change*, *17*(7), 2039–2053. <https://doi.org/10.1007/s10113-016-0996-1>

- 546 Chalov, S., Bazilova, V., Tarasov, M. (2017b). Suspended sediment balance in Selenga Delta at
547 the Late XX–Early XXI Century: Simulation by LANDSAT satellite smages. *Water*
548 *Resources* Vol. 44, No. 3, pp. 463–470. <https://doi.org/10.1134/S0097807817030071>
- 549 Chini, M., Hostache, R., Giustarini, L., & Matgen, P. (2017). A hierarchical split-based approach
550 for parametric thresholding of SAR images: Flood inundation as a test case. *IEEE*
551 *Transactions on Geoscience and Remote Sensing*, 55(12), 6975–6988.
552 <https://doi.org/10.1109/TGRS.2017.2737664>
- 553 Crétaux, J.-F., Jelinski, W., Calmant, S., Kouraev, A., Vuglinski, V., Bergé-Nguyen, M., et al.
554 (2011). SOLS: A lake database to monitor in the Near Real Time water level and storage
555 variations from remote sensing data. *Advances in Space Research*, 47(9), 1497–1507.
556 <https://doi.org/10.1016/j.asr.2011.01.004>
- 557 Cui, Y., Xiao, R., Zhang, M., Wang, C., Ma, Z., Xiu, Y., Wang, Q. and Guo, Y. (2020).
558 Hydrological connectivity dynamics and conservation priorities for surface-water patches
559 in the Yellow River Delta National Nature Reserve, China. *Ecohydrology &*
560 *Hydrobiology*. <https://doi.org/10.1016/j.ecohyd.2020.03.005>
- 561 Donchyts, G., Baart, F., Winsemius, H., Gorelick, N., Kwadijk, J., & Van De Giesen, N. (2016).
562 Earth’s surface water change over the past 30 years. *Nature Climate Change*, 6(9), 810–
563 813. <https://doi.org/10.1038/nclimate3111>
- 564 Dong, T. Y., Nittrouer, J. A., Czapiga, M. J., Ma, H., McElroy, B., Il’icheva, E, Pavlov M,
565 Chalov S, Parker G. (2019). Roles of bank material in setting bankfull hydraulic
566 geometry as informed by the Selenga River delta, Russia. *Water Resources Research*
567 Volume 55, Issue 1, pp. 827-846. <https://doi.org/10.1029/2017WR021985>
- 568 Garmaev, E.Z., Kulikov, A.I., Tsydypov, B.Z., Sodnomov, B. V., Ayurzhanayev, A.A. (2019).
569 Environmental conditions of Zakamensk Town (Dzhida River Basin Hotspot).
570 *Geography, Environment, Sustainability*, 12(3), pp.224-239.
571 <https://doi.org/10.24057/2071-9388-2019-32>
- 572 Gelfan, A.N., Millionshchikova, T.D. (2018). Validation of a hydrological model intended for
573 impact study: Problem statement and solution example for Selenga River Basin. *Water*
574 *Resources*, 45, 90–101. <https://doi.org/10.1134/S0097807818050354>
- 575 Ghajarnia, N., Destouni, G., Thorslund, J., Kalantari, Z., Åhlén, I., Anaya-Acevedo, J.A.,
576 Blanco-Libreros, J.F., Borja, S., Chalov, S., Chun, K.P., Desormeaux, A., Garfield, B.,

- 577 Hansen, A., Jaramillo, F., Jarsjö, J., Labbaci, A., Livsey, J., Maneas, G., McCurley, K.,
578 Palomino-Ángel, S., Pietron, J., Price, R., Monroy, V.R., Salgado, J., Sannel, B.,
579 Seifollahi-Aghmiuni, S., Sjöberg, Y., Tersky, P., Vigouroux, G., Villanueva, L.L. (2020).
580 Data for wetlandscapes and their changes around the world. *Earth System Science Data*,
581 12(2), pp.1083-1083. <https://doi.org/10.5194/essd-12-1083-2020>
- 582 Giesen, N. van de. (2020). Human activities have changed the shapes of river deltas. *Nature*,
583 577(7791), 473–474. <https://doi.org/10.1038/d41586-020-00047-y>
- 584 Golden, H. E., Lane, C. R., Amatya, D. M., Bandilla, K. W., Raanan Kiperwas, H., Knightes, C.
585 D., & Ssegane, H. (2014). Hydrologic connectivity between geographically isolated
586 wetlands and surface water systems: A review of select modeling methods.
587 *Environmental Modelling & Software*, 53, 190–206.
588 <https://doi.org/10.1016/j.envsoft.2013.12.004>
- 589 Guo, M., Li, J., Sheng, C., Xu, J., & Wu, L. (2017). A review of wetland remote sensing.
590 *Sensors*, 17(4), 777. <https://doi.org/10.3390/s17040777>
- 591 Hulme, M. (1992). A 1951–80 global land precipitation climatology for the evaluation of general
592 circulation models. *Climate Dynamics*, 7(2), 57–72. <https://doi.org/10.1007/BF00209609>
- 593 Hulme, M., Osborn, T. J., & Johns, T. C. (1998). Precipitation sensitivity to global warming:
594 Comparison of observations with HadCM2 simulations. *Geophysical Research Letters*,
595 25(17), 3379–3382. <https://doi.org/10.1029/98GL02562>
- 596 Jaramillo, F., Brown, I., Castellazzi, P., Espinosa, L., Guittard, A., Hong, S.-H., et al. (2018).
597 Assessment of hydrologic connectivity in an ungauged wetland with InSAR observations.
598 *Environmental Research Letters*, 13(2), 024003. <https://doi.org/10.1088/1748-9326/aa9d23>
- 600 Jarsjö J, Chalov S, Pietron J, Alekseenko A, Thorslund J. (2017). Patterns of soil contamination,
601 erosion, and river loading of metals in a gold mining region of Northern Mongolia.
602 *Regional Environmental Change*, 17(7): 1991-2005. <https://doi.org/10.1007/s10113-017-1169-6>
- 603 1169-6
- 604 Lane, C. R., Liu, H., Autrey, B. C., Anenkhonov, O. A., Chepinoga, V. V., & Wu, Q. (2014).
605 Improved wetland classification using eight-band high resolution satellite imagery and a
606 hybrid approach. *Remote Sensing*, 6(12), 12187–12216.
607 <https://doi.org/10.3390/rs61212187>

- 608 Lane, C. R., Anenkhonov, O., Liu, H., Autrey, B. C., & Chepinoga, V. (2015). Classification and
609 inventory of freshwater wetlands and aquatic habitats in the Selenga River Delta of Lake
610 Baikal, Russia, using high-resolution satellite imagery. *Wetlands Ecology and
611 Management*, 23(2), 195–214. <https://doi.org/10.1007/s11273-014-9369-z>
- 612 Lu, Z., & Kwoun, O. i. (2008). Radarsat-1 and ERS InSAR analysis over Southeastern coastal
613 Louisiana: Implications for mapping water-level changes beneath swamp forests. *IEEE
614 Transactions on Geoscience and Remote Sensing*, 46(8), 2167–2184.
615 <https://doi.org/10.1109/TGRS.2008.917271>
- 616 Masek, J. G., Vermote, E. F., Saleous, N. E., Wolfe, R., Hall, F. G., Huemmrich, K. F., et al.
617 (2006). A Landsat surface reflectance dataset for North America, 1990-2000. *IEEE
618 Geoscience and Remote Sensing Letters*, 3(1), 68–72.
619 <https://doi.org/10.1109/LGRS.2005.857030>
- 620 McFeeters, S. K. (1996). The use of the Normalized Difference Water Index (NDWI) in the
621 delineation of open water features. *International Journal of Remote Sensing*, 17(7),
622 1425–1432. <https://doi.org/10.1080/01431169608948714>
- 623 Moragoda, N., & Cohen, S. (2020). Climate-induced trends in global riverine water discharge
624 and suspended sediment dynamics in the 21st century. *Global and Planetary Change*,
625 191, 103199. <https://doi.org/10.1016/j.gloplacha.2020.103199>
- 626 Nguyen Thanh, T., Tri, V.P.D., Kim, S., Phuong, T.N., Mong, T.L. and Tuan, P.V. (2020). A
627 subregional model of system dynamics research on surface water resource assessment for
628 paddy rice production under climate change in the Vietnamese Mekong Delta. *Climate*,
629 8(3), p.41. <https://doi.org/10.3390/cli8030041>
- 630 Nienhuis, J. H., Ashton, A. D., Edmonds, D. A., Hoitink, A. J. F., Kettner, A. J., Rowland, J. C.,
631 & Törnqvist, T. E. (2020). Global-scale human impact on delta morphology has led to net
632 land area gain. *Nature*, 577(7791), 514–518. <https://doi.org/10.1038/s41586-019-1905-9>
- 633 Palomino-Ángel, S., Anaya-Acevedo, J.A., Simard, M., Liao, T.H. and Jaramillo, F. (2019).
634 Analysis of floodplain dynamics in the Atrato River Colombia using SAR
635 interferometry. *Water*, 11(5), p.875. <https://doi.org/10.3390/w11050875>
- 636 Pekel, J.-F., Cottam, A., Gorelick, N., & Belward, A. S. (2016). High-resolution mapping of
637 global surface water and its long-term changes. *Nature*, 540(7633), 418.
638 <https://doi.org/10.1038/nature20584>

- 639 Pietron, J., Nittrouer, J.A., Chalov, S.R.; Dong, T.Y., Kasimov, N., Shinkareva, G., Jarsjö, J.
640 (2018). Sedimentation patterns in the Selenga River Delta under changing hydroclimatic
641 conditions. *Hydrological processes*, 32(2), pp.278-292.
642 <https://doi.org/10.1002/hyp.11414>
- 643 Potemkina, T. G. (2011). Sediment runoff formation trends of major tributaries of Lake Baikal in
644 the 20th century and at the beginning of the 21st century. *Russian Meteorology and*
645 *Hydrology*, 36(12), 819–825. <https://doi.org/10.3103/S1068373911120077>
- 646 Richards, J. A. (1999). Remote sensing digital image analysis (Vol. 3). Springer. Retrieved from
647 DOI 10.1007/978-3-642-30062-2
- 648 Shinkareva G.L., Lychagin M.Y., Tarasov M.K., Pietron J., Chichaeva M.A., Chalov S.R.
649 (2019). Biogeochemical specialization of macrophytes and their role as a biofilter in the
650 Selenga Delta. *Geography, Environment, Sustainability*, 10, pp.2071-9388.
651 <https://doi.org/10.24057/2071-9388-2019-103>
- 652 Syvitski, J. P., Kettner, A. J., Overeem, I., Hutton, E. W., Hannon, M. T., Brakenridge, G. R., et
653 al. (2009). Sinking deltas due to human activities. *Nature Geoscience*, 2(10), 681–686.
654 <https://doi.org/10.1038/ngeo629>
- 655 Tapley, B., Ries, J., Bettadpur, S., Chambers, D., Cheng, M., Condi, F., Gunter, B., Kang, Z.,
656 Nagel, P., Pastor, R. and Pekker, T. (2005). GGM02—An improved Earth gravity field
657 model from GRACE. *Journal of Geodesy*, 79(8), pp.467-478. DOI 10.1007/s00190-005-
658 0480-z
- 659 Vermote, E., Justice, C., Claverie, M., & Franch, B. (2016). Preliminary analysis of the
660 performance of the Landsat 8/OLI land surface reflectance product. *Remote Sensing of*
661 *Environment*, 185, 46–56. <https://doi.org/10.1016/j.rse.2016.04.008>
- 662 Zhang, G., Yao, T., Piao, S., Bolch, T., Xie, H., Chen, D., et al. (2017). Extensive and drastically
663 different alpine lake changes on Asia’s high plateaus during the past four decades.
664 *Geophysical Research Letters*, 44(1), 252–260. <https://doi.org/10.1002/2016GL072033>
- 665 Zhou, Y., Dong, J., Xiao, X., Xiao, T., Yang, Z., Zhao, G., et al. (2017). Open surface water
666 mapping algorithms: A comparison of water-related spectral indices and sensors. *Water*,
667 9(4), 256. <https://doi.org/10.3390/w9040256>

668

669

Temporal and Spatial Changes of Water Occurrence in the Selenga River Delta

Saeid Aminjafari¹, Ian A. Brown¹, Sergey R. Chalov², Marc Simard³, Jerker Jarsjö¹, Mehdi Darvishi¹, Fernando Jaramillo^{1,4}

¹Department of Physical Geography and Bolin Centre for Climate Research, Stockholm University, SE-106 91, Stockholm, Sweden.

²Faculty of Geography, Lomonosov Moscow State University, 119991 Moscow, Russia.

³Radar Science and Engineering Section, NASA Jet Propulsion Laboratory, USA.

⁴Baltic Sea Centre and Stockholm Resilience Center, Stockholm University, SE-106 91 Stockholm, Sweden.

Contents of this file

Tables S1 to S6

Introduction

We applied two classifiers on four images in two conditions; one considering all bands of the Landsat products without any indices, and another one by considering the combination of NDWI, NDVI, NIR, SWIR2, and Blue band. Tables S1 to S4 show that the band-index combination leads to higher accuracy.

Image 1987-09-25		All bands included	Selected Bands and indices combination
Maximum Likelihood	Overall accuracy (%)	99.1566	99.5689
	Kappa Coefficient	0.9536	0.9767

Table S1. Classification accuracy for Landsat image 1987/09/25

Image 1995-09-15		All bands included	Selected Bands and indices combination
Maximum Likelihood	Overall accuracy (%)	98.5446	98.9877
	Kappa Coefficient	0.9208	0.9461

Table S2. Classification accuracy for Landsat image 1995/09/15

Image 2005-09-26		All bands included	Selected Bands and indices combination
Maximum Likelihood	Overall accuracy (%)	99.6863	99.8201
	Kappa Coefficient	0.9753	0.9860

Table S3. Classification accuracy for Landsat image 2005/09/26

Image 2018-09-30		All bands included	Selected Bands and indices combination
Maximum Likelihood	Overall accuracy (%)	98.6579	98.8823
	Kappa Coefficient	0.8971	0.9129

Table S4. Classification accuracy for Landsat image 2018/09/30

	Jan	Feb	Mar	Apr	May	Jun	Jul	Aug	Sep	Oct	Nov	Dec
1987									25			
1988												
1989						18		21	30			
1990												
1991												
1992											09	
1993												
1994									12			

1995								14,30	15	01		
1996			26		13	31			01			
1997			13					03,19	20		07	
1998			16		03	05		22				
1999				05	22			25	26			
2000					24			11				
2001			24	10	27	29					02,18	
2002			11	13					18			
2003								04				
2004							05		07	25	26	
2005			03,19						26			
2006					25			28				
2007				27								
2008										04		
2009			14									
2010					20	06	23			10		
2011					07				11			
2012												
2013								31		02,18	03	
2014			12,28	30		17				21	06	
2015		30			02,18	20	21	06				
2016												
2017					23	09			11	29		
2018			07	09				13,29	30	16		
2019			10	12	13			16				

Table S5. The number of images used in the study per year. The numbers in each cell show the day of the column month.

Land Cover	No Pixels with $\overline{\Delta w} \neq 0$	Total No of Pixels
CFDNL	8201	9386
CFN	48533	52925
Herb	261683	334843
OFDNL	951	1143
OFN	138628	147202
Sand Bar	2007	2046
Shrub	3894	3929
Wetland	73872	78084
Permanent Water	107903	592437
Seasonal Water	250194	252062
Land	338522	522034

Total	696621	1366533
-------	--------	---------

Table S6. Number of Pixels per landcover. The abbreviations correspond to the names in Figure 4 in the manuscript.